Tellus (1994), 46A, 14–33
Printed in Belgium – all rights reserved

TELLUS
ISSN 0280–6495

Cyclogenesis in a conditionally unstable moist baroclinic atmosphere

By MANKIN MAK, *Department of Atmospheric Sciences, U. of Illinois at Urbana-Champaign, Urbana, IL 61801, USA*

(Manuscript received 1 December 1992; in final form 26 July 1993)

ABSTRACT

This paper reports the analytic solution of the instability problem of a conditionally unstable moist baroclinic basic flow for a general heating profile and the quantitative results for the special case of a uniform heating profile. There are 4 discrete eigenmodes arising from the existence of potential vorticity (PV) anomalies at only 4 discrete vertical levels in this generic model setting. There is one unstable mode for a weak to moderate heating. The growth rate and wavelength of the most unstable moist Eady mode have a strongly nonlinear dependence on the heating intensity in this range. Significant enhancement in the growth rate and reduction in the wavelength of this mode are found when the heating intensity is increased to a moderate value. The trends of variation of these instability properties with the heating intensity are reversed for stronger heating due to a strong interference of the interactions among the PV anomalies at the four levels. The phase velocity of this mode is affected relatively little by the condensational heating. For a moderate to strong heating, there are two new branches of shorter unstable modes. The modes of one branch have a large phase velocity and are largely confined between the model tropopause and the top of the heating layer. They primarily arise from the interaction of the PV anomalies at those 2 levels. The modes of the other branch are largely confined between the model surface and the bottom of the heating layer with a small phase velocity arising from a similar dynamical origin. The self-induced heating and the basic baroclinic shear are jointly responsible for the existence of these modes. These 2 branches of mode may coexist. The energetic of the unstable modes is consistent with such a dynamical interpretation.

1. Introduction

The importance of condensational heating for the development of the vigorous storms in the extratropics is fairly well established. A number of storms that have been under close scrutiny are all found to be strongly energized by the released latent heat. Their development rate, their structure, and their movement are noticeably influenced by the condensational heating (e.g., Gyakum, 1983; Whitaker et al., 1988; Hoskins and Berrisford, 1988; Kristjansson, 1990).

One approach of investigating the role of latent heating is by means of numerical simulation of an actual storm with a state-of-the-art model. A comparison of the development of the same storm with versus without the condensational heating in a model would quantify the impact of the heating. According to a recent simulation study of the famous QE-II storm over ocean by Kuo et al. (1991), the dry model predicts a deepening of only 11 mb (1004–993 mb) of surface pressure in 24 hrs and the moist model predicts a deepening of 37 mb (1004–967 mb). The observed deepening could be actually as much as 59 mb (1004–945 mb). In other words, the condensational heating could increase the intensification of the storm by a factor of 3 to 5. The simulation also suggests that the heating rate may be as large as a few hundred degrees per day in a fairly thick layer. Even a relatively small storm over northern Europe in August is found to have more than 10 cm of precipitation in 24 h and is confined largely in the lower troposphere with a surface wind exceeding

25 ms^{-1} (Grønås et al., 1992). Both simulations agree reasonably well with observation.

Since the details of the precipitation process are very complex and occur on scales much shorter than any model can explicitly represent, the latent heating has to be parameterized in one way or the other. The form of parameterization has been naturally a subject of controversy which is unlikely to be resolved for sometime in a truly definitive manner. The worthiness of a scheme is often pragmatically judged by how well the storm could be simulated with the use of it. For example, Grønås et al. (1992) found that their simulation would not be comparable to observation unless they incorporated Sundqvist's scheme (Sundquist et al., 1989) which embodies Kuo's (1974) convective condensation scheme as one of its many components. There have been also a number of numerical model studies using idealized basic flows and various parameterization schemes in different model settings (Gall, 1976; Sardie and Warner, 1983; Moorthi and Arakawa, 1985; Bonatti and Rao, 1987; Craig and Cho, 1992).

It warrants to use a much simpler parameterization scheme in a theoretical study in the hope of ascertaining the essence of the dynamical process. Two substantially different types of idealized schemes have been applied. One type rests upon the notion that the effect of the condensational heating might be represented in a model in the form of a reduced static stability at all levels in the region of ascending motion (e.g., Bennets and Hoskins, 1979; Tang and Fichtl, 1983; Emanuel et al., 1987; Fantini, 1993). This scheme assumes that ascending air at all levels is saturated. The heating rate is calculated assuming that a rising air parcel conserves its equivalent potential temperature. The results suggest that the latent heating would increase the growth rate by about a factor of two and that the width of the ascending region is much narrower than the descending region in the context of an Eady model. This scheme probably serves to represent the large scale latent heat release.

The other type of parameterization scheme used in some theoretical studies is based on the concept of Conditional Instability of the Second Kind (CISK, Charney and Eliassen, 1964; Ooyama, 1964). This scheme would be applicable when the interior of the atmospheric domain under consideration is unsaturated but conditionally unstable due to the presence of a significant surface moist layer. CISK is a notion that a large scale disturbance and the ensemble of clouds embedded in it could amplify together as a result of cooperative interaction between them. This general concept is meaningful as long as the large scale disturbance under consideration has an inherent field of convergence and divergence with significant values near the surface where most moisture resides. One might add that CISK-like development is found in storms which are modeled with a much more complex parameterization scheme (e.g., Grønås et al., 1992).

For the problem of extratropical cyclogenesis, the basic shear is also expected to play an important role. Therefore, a dynamical problem worthy of a thorough investigation is that of moist baroclinic instability of a simple basic flow in the context of a wave-CISK model. There have been several studies of this type (Mak, 1982; Bannon, 1986; Craig and Cho, 1988; and Wang and Barcilon, 1986; Snyder and Lindzen, 1991). The last study just cited uses a model unbounded above and below in order to demonstrate how the heating may trigger instability by means of redistributing the potential vorticity. While that study serves to highlight this dynamical role of the heating in a simplest possible setting, the neglect of the earth's surface and tropopause in a model is much too drastic. Considering the relative thicknesses of the troposphere, the heating layer and the surface moist layer in conjunction with the vertical extent of a typical storm, it is not justifiable to ignore the influence of the boundaries either by means of a heuristic scale analysis or a systematic perturbation analysis. The earth's surface and tropopause in the presence of a baroclinic shear do in fact play an important and essential dynamical role in moist cyclogenesis as we will see from the results of this analysis.

The author's earlier investigation (Mak, 1982) was performed with an assumption which is only justifiable when the heating is weak. The objective of this study is to generalize the analysis by revoking that assumption. This analysis only invokes the hypothesis that the heating rate is linearly proportional to the vertical velocity at the top of a moist layer. The new findings are considerably more general. Furthermore, all results can be unambiguously interpreted from the potential vorticity point of view as one would expect in

light of the general discussion of Haynes and McIntyre (1987). In Section 2, I will first present an analytic investigation of this problem for a general heating profile. The general formulae for both the eigenvalue and eigenfunctions are next applied to a special case of a uniform heating profile in order to evaluate a complete set of quantitative results, including the energetic. The results and their interpretations are presented in Section 3.

2. Model and analysis

2.1. Basic equations

The extratropical atmosphere typically has a well-defined baroclinic zone between the tropopause and the surface. Therefore the simplest meaningful model for moist cyclogenesis to consider is a two-dimensional Eady model with a surface layer of moisture allowing for a self-induced condensational heating by a disturbance itself. The governing perturbation equations in such a model are the vorticity equation and the thermodynamic equation incorporating the geostrophic and hydrostatic balances. In pressure coordinates, they are:

$$\left(\frac{\partial}{\partial t}+\bar{u}\frac{\partial}{\partial x}\right)\frac{\partial^2\psi}{\partial x^2}=f\frac{\partial\omega}{\partial p}, \tag{1}$$

$$\left(\frac{\partial}{\partial t}+\bar{u}\frac{\partial}{\partial x}\right)\frac{\partial\psi}{\partial p}-\frac{\mathrm{d}\bar{u}}{\mathrm{d}p}\frac{\partial\psi}{\partial x}=-\frac{S}{f}\omega-\frac{RQ}{fp}, \tag{2}$$

where the notations are standard: (x, p, t) stand for (zonal coordinate, pressure, time), f = Coriolis parameter,

$$S=-\frac{R}{p}\left(\frac{\partial T_0}{\partial p}-\frac{RT_0}{c_p p}\right)$$

= basic static stability ($\mathrm{m^2\,s^{-2}\,mb^{-2}}$),

and R = gas constant, c_p = specific heat at constant pressure, T_0 = horizontal domain average background temperature. The unknowns are the perturbation streamfunction, ψ and perturbation vertical velocity, ω. Q is the condensational heating rate ($\mathrm{K\,s^{-1}}$).

The Eady model has a constant static stability S and a basic flow with a constant vertical shear,

$$\bar{u}=\lambda(p_{00}-p), \tag{3}$$

where λ is a parameter for the shear. The domain under consideration is

$$0\leqslant x\leqslant\infty, \qquad p_1<p<p_\infty.$$

The horizontal distance, velocity, time and pressure may be measured in units of L, U, LU^{-1}, and p_{00}, respectively. The analysis is made in terms of the nondimensional quantities defined below.

$$x'=\frac{x}{L}, \qquad t'=\frac{Ut}{L}, \qquad p'=\frac{p}{p_{00}},$$

$$\psi'=\frac{\psi}{UL}, \qquad \omega'=\frac{\omega L^2 f}{U^2 p_{00}}, \qquad \bar{u}=\frac{\bar{u}}{U},$$

$$S'=S\left(\frac{p_{00}}{fL}\right)^2, \qquad \lambda'=\frac{\lambda p_{00}}{U}, \qquad Q'=\frac{QR}{fU^2}.$$

Then the non-dimensional form of eqs. (1) and (2) may be written as (dropping the prime).

$$\left(\frac{\partial}{\partial t}+\bar{u}\frac{\partial}{\partial x}\right)\frac{\partial^2\psi}{\partial x^2}=\frac{\partial\omega}{\partial p}, \tag{4}$$

$$\left(\frac{\partial}{\partial t}+\bar{u}\frac{\partial}{\partial x}\right)\frac{\partial\psi}{\partial p}+\lambda\frac{\partial\psi}{\partial x}=-S\omega-\frac{Q}{p}, \tag{5}$$

with $\bar{u}=\lambda(1-p)$. The domain is $0\leqslant x\leqslant\infty$, $p_1\leqslant p\leqslant 1$. The vertical boundary conditions are:

$$\omega=0, \qquad \text{at} \quad p=p_1, 1 \tag{6}$$

implying

$$\left(\frac{\partial}{\partial t}+\bar{u}\frac{\partial}{\partial x}\right)\frac{\partial\psi}{\partial p}+\lambda\frac{\partial\psi}{\partial x}=0, \tag{7}$$

because we may assume no heating at the model boundaries $p=p_1$ and 1. It is more convenient to work with the two equivalent equations which are readily derivable from (4) and (5). They are the so-called omega-equation and potential vorticity equation.

$$\frac{\partial^2\omega}{\partial p^2}+S\frac{\partial^2\omega}{\partial x^2}=-2\lambda\frac{\partial^3\psi}{\partial x^3}-\frac{\partial^2}{\partial x^2}\left(\frac{Q}{p}\right), \tag{8}$$

$$\left(\frac{\partial}{\partial t}+\bar{u}\frac{\partial}{\partial x}\right)\left(S\frac{\partial^2\psi}{\partial x^2}+\frac{\partial^2\psi}{\partial p^2}\right)=-\frac{\partial}{\partial p}\left(\frac{Q}{p}\right). \tag{9}$$

It is instructive to emphasize that, according to (9), the perturbation potential vorticity would be increased where the latent heating (more precisely, where Q/p) increases with height and vice versa. Hence, the microphysics of clouds influences the character of the large scale dynamics through its direct impacts on the vertical profile of the heating. We can also readily infer from (8) that a heating ($Q>0$) would have a positive feedback influence on the ascending motion ($\omega<0$).

2.2. *Treatment of the condensational heating*

In accordance with the concept of CISK, let us assume that when the vertical velocity of a large scale disturbance transports moisture out of the moist layer, the condensational process would take place, the released latent heat would be distributed vertically according to a certain heating profile, and the liquid water would precipitate out of the atmospheric column. Since a baroclinic wave disturbance intrinsically has a vertical velocity field, a self-induced heating could take place even without considering the surface frictional effect. A large-scale disturbance therefore may cooperatively interact with an ensemble of clouds embedded in it. We therefore, assume the heating rate to be proportional to $-\omega$ at the top of the moist layer, p_B, where ω_B is negative, and is zero where $\omega_B>0$. The vertical distribution of the released heat is controlled by a heating profile function $\hat{h}(p)$. The proportionality constant may be regarded as being proportional to the specific humidity in the surface moist layer. In non-dimensional form, we therefore write the heating rate as

$$Q=\begin{cases}-\varepsilon\hat{h}(p)\,\omega_B, & \text{for}\quad \omega_B<0\\ 0 & \text{otherwise}\end{cases} \tag{10}$$

where $\varepsilon=(Rp_{00}/f^2L^2)\,\varepsilon_{\text{dim}}$ is referred to as the heating intensity parameter. It should be stressed that ε by itself does not tell us about the heating intensity for ω_B is part of the unknown solution.

The positive definite nature of the heating naturally leads to a coupling among the different wave components in a perturbation. It can be readily shown in a Fourier decomposition that for

$$\omega_B=\int_{-\infty}^{\infty}W_B(k)\,e^{ikx}\,dk \tag{11}$$

we have

$$Q=\int_{-\infty}^{\infty}\tilde{Q}(k,p)\,e^{ikx}\,dk \tag{12}$$

where

$$\tilde{Q}(k,p)=-\frac{\varepsilon}{2}\hat{h}(p)\,W_B(k)+\text{coupling term}. \tag{13}$$

The coupling term is an integral involving other spectral components $W_B(m)$, $m\neq k$. We will further apply the approximation of linearization that the heating induced by a wave disturbance has the strongest feedback effect on itself. It would take an extensive numerical analysis to ascertain the quantitative influence of the coupling term. As it lies beyond the scope of this study, it is best left to a future study. Specifically, we approximate (13) as

$$\tilde{Q}(k;p)=-\frac{\varepsilon\hat{h}}{2}W_B(k). \tag{14}$$

It is noted in passing that the factor $\frac{1}{2}$ in (14) was not included in some earlier studies (e.g., Mak, 1982; Wang and Barcilon, 1986). This factor needs to be taken into account when we make a comparison of the counterpart results later in the next section. We may then examine each wave mode of the solution separately in the form of

$$(\omega,\psi)=\text{Re}\,[(W(p),\Psi(p))\,e^{i(kx-\sigma t)}]. \tag{15}$$

It follows from (7), (8) and (14) that the amplitude functions of a normal mode (15) are governed by

$$\frac{d^2W}{dp^2}-Sk^2W=i2\lambda k^3\Psi-\frac{\varepsilon k^2}{2}hW_B, \tag{16}$$

$$i(\bar{u}k-\sigma)\left(\frac{d^2\Psi}{dp^2}-Sk^2\Psi\right)=\frac{\varepsilon}{2}W_B\frac{dh}{dp} \tag{17}$$

$$\text{at}\quad p=p_1,\,1,\qquad W=0, \tag{18a}$$

$$(\bar{u}k-\sigma)\frac{d\Psi}{dp}+\lambda k\Psi=0, \tag{18b}$$

where $h=\hat{h}(p)/p$ is simply referred to for convenience as the heating profile.

Tellus A/46/1-2

2.3. Analysis with a general heating profile

The following methodology is used for solving the eigenvalue-eigenfunction problem defined by eqs. (16) and (17) subject to the boundary conditions (18a, b) with σ being the eigenvalue. They are first transformed to a single integral equation by repeatedly applying the method of Green's function. This leads to a Fredholm equation with a degenerate kernel. We will see that this approach can be applied without introducing any further approximation from this point on.

To begin with, we obtain from (16) an integral relation between W and Ψ which satisfies (18a) by applying the method of Green's function, viz.

$$W=\int_{p_1}^{1} G(p,\tilde{p})\left[i2\lambda k^3\Psi(\tilde{p})-\frac{\varepsilon k^2}{2}W_{\mathrm{B}}h(\tilde{p})\right]\mathrm{d}\tilde{p}, \tag{19}$$

where the Green function is

$$G(p,\tilde{p})=\begin{cases} G_1(p,\tilde{p})=\dfrac{1}{a}\eta(\tilde{p})\,\xi(p), & \text{for} \quad p<\tilde{p},\\ G_2(p,\tilde{p})=\dfrac{1}{a}\eta(p)\,\xi(\tilde{p}), & \text{for} \quad p>\tilde{p},\end{cases}$$

$$\begin{aligned}&\xi(p)=\mathrm{e}^{m(p-p_1)}-\mathrm{e}^{-m(p-p_1)},\\ &\eta(p)=\mathrm{e}^{m(p-1)}-\mathrm{e}^{-m(p-1)},\\ &a=-2m\eta(p_1),\\ &m=k\sqrt{S}.\end{aligned} \tag{20}$$

We now apply (19) at the level $p=p_{\mathrm{B}}$ and obtain:

$$W_{\mathrm{B}}=\frac{i2\lambda k^3\int_{p_1}^{1} G(p_{\mathrm{B}},\tilde{p})\,\Psi(\tilde{p})\,\mathrm{d}\tilde{p}}{1+\dfrac{\varepsilon k^2}{2}\displaystyle\int_{p_1}^{1} G(p_{\mathrm{B}},\tilde{p})\,h(\tilde{p})\,\mathrm{d}\tilde{p}}. \tag{21}$$

Substituting (21) into (17) would then lead to a differential-integral equation for Ψ alone.

$$\frac{\mathrm{d}^2\Psi}{\mathrm{d}p^2}-Sk^2\Psi = \frac{\varepsilon\lambda k^3\dfrac{\mathrm{d}h}{\mathrm{d}p}\displaystyle\int_{p_1}^{1} G(p_{\mathrm{B}},\tilde{p})\,\Psi(\tilde{p})\,\mathrm{d}\tilde{p}}{(\bar{u}k-\sigma)\left(1+\dfrac{\varepsilon k^2}{2}\right)\displaystyle\int_{p_1}^{1} G(p_{\mathrm{B}},\tilde{p})\,h(\tilde{p})\,\mathrm{d}\tilde{p}}.$$

This equation can be further transformed to an integral equation by applying the method of the Green function one more time. This yields

$$\Psi(p)=\frac{\lambda k^3\varepsilon\displaystyle\int_{p_1}^{1}\frac{K(p,\tilde{p})}{\bar{u}(\tilde{p})\,k-\sigma}\frac{\mathrm{d}h(\tilde{p})}{\mathrm{d}\tilde{p}}\mathrm{d}\tilde{p}}{1+\dfrac{\varepsilon k^2}{2}\displaystyle\int_{p_1}^{1} G(p_{\mathrm{B}},\tilde{p})\,h(\tilde{p})\,\mathrm{d}\tilde{p}} \times\int_{p_1}^{1} G(p_{\mathrm{B}},\tilde{p})\,\Psi(\tilde{p})\,\mathrm{d}\tilde{p}, \tag{22}$$

where the second Green function is

$$K(p,\tilde{p})=\begin{cases} K_1(p,\tilde{p})=\dfrac{1}{b}\theta(\tilde{p})\,\gamma(p), & \text{for} \quad p<\tilde{p},\\ K_2(p,\tilde{p})=\dfrac{1}{b}\theta(p)\,\gamma(\tilde{p}), & \text{for} \quad p>\tilde{p},\end{cases}$$

$$\begin{aligned}&\gamma(p)=\mathrm{e}^{m(p-p_1)}+\left(\frac{\sigma-\bar{u}_1k-\tilde{\lambda}}{\sigma-\bar{u}_1k+\tilde{\lambda}}\right)\mathrm{e}^{-m(p-p_1)},\\ &\theta(p)=\mathrm{e}^{m(p-1)}+\left(\frac{\sigma-\tilde{\lambda}}{\sigma+\tilde{\lambda}}\right)\mathrm{e}^{-m(p-1)},\\ &b=2m\left[\left(\frac{\sigma-\bar{u}_1k-\tilde{\lambda}}{\sigma-\bar{u}_1k+\tilde{\lambda}}\right)\mathrm{e}^{m(p_1-1)}-\left(\frac{\sigma-\tilde{\lambda}}{\sigma+\tilde{\lambda}}\right)\mathrm{e}^{-m(p_1-1)}\right],\\ &\tilde{\lambda}=\frac{\lambda}{\sqrt{S}}.\end{aligned} \tag{23}$$

Note that the $K(p,\tilde{p})$ satisfies the boundary conditions (18b).

Eq. (22) is a Fredholm equation. The important point to note is that (22) has a degenerate kernel. Multiplying (22) by $G(p_{\mathrm{B}},p)$, integrating the resulting eq. over the domain, and after cancelling the common factor, $\int_{p_1}^{1} G(p_{\mathrm{B}},\tilde{p})\,\Psi(\tilde{p})\,\mathrm{d}\tilde{p}$, from both sides, we finally obtain,

$$\begin{aligned}&1+\frac{\varepsilon k^2}{2}\int_{p_1}^{1} G(p_{\mathrm{B}},\tilde{p})\,h(\tilde{p})\,\mathrm{d}\tilde{p}\\ &\quad=\lambda k^3\varepsilon\int_{p_1}^{1}\left(\int_{p_1}^{1}\frac{K(p,\tilde{p})}{\bar{u}(\tilde{p})\,k-\sigma}\frac{\mathrm{d}h(\tilde{p})}{\mathrm{d}\tilde{p}}\mathrm{d}\tilde{p}\right)\\ &\quad\times G(p_{\mathrm{B}},p)\,\mathrm{d}p.\end{aligned} \tag{24}$$

This is a general necessary condition for the existence of a non-trivial normal mode solution. It can be used to determine the eigenvalue, σ, for any

heating profile, h. We may further analytically carry out the integration in (24) if the prescribed heating profile h is a sufficiently simple function of p. This will be done in the next subsection.

The analytic expressions for the eigenfunction in terms of W and Ψ may be deduced as follows. It is noted that the integral relation (22) has the following form:

$$M(p)\,\Psi(p)=\int_{p_1}^{1} G(p_B,\tilde{p})\,\Psi(\tilde{p})\,\mathrm{d}\tilde{p}. \tag{25}$$

where

$$M(p)=\frac{1+\dfrac{\varepsilon k^2}{2}\displaystyle\int_{p_1}^{1} G(p_B,\tilde{p})\,h(\tilde{p})\,\mathrm{d}\tilde{p}}{\lambda k^3\varepsilon\displaystyle\int_{p_1}^{1}\frac{K(p,\tilde{p})}{\bar{u}(\tilde{p})\,k-\sigma}\frac{\mathrm{d}h(\tilde{p})}{\mathrm{d}\tilde{p}}\,\mathrm{d}\tilde{p}}. \tag{26}$$

It is useful to note that the r.h.s. of (25) is a quantity independent of p whatever the solution $\Psi(p)$ might be. It follows that while M and Ψ individually varies with p, their product does not. Hence we may write

$$M(p)\,\Psi(p)=M(1)\,\Psi(1). \tag{27}$$

Furthermore, we may set $\Psi(1)=1$ as a normalization constant without loss of generality. Then the solution for Ψ is simply

$$\Psi(p)=\frac{\displaystyle\int_{p_1}^{1}\frac{K(p,\tilde{p})}{\bar{u}(\tilde{p})\,k-\sigma}\frac{\mathrm{d}h(\tilde{p})}{\mathrm{d}\tilde{p}}\,\mathrm{d}\tilde{p}}{\displaystyle\int_{p_1}^{1}\frac{K(1,\tilde{p})}{\bar{u}(\tilde{p})\,k-\sigma}\frac{\mathrm{d}h(\tilde{p})}{\mathrm{d}\tilde{p}}\,\mathrm{d}\tilde{p}}. \tag{28}$$

Thus, once an eigenvalue σ is known by solving (24), we can use it together with (28) to determine the structure of the corresponding eigenfunction for $\Psi(p)$.

Now, (25), (26), and (27) in turn enable us to rewrite (21) as

$$W_B=\frac{i2}{\varepsilon\displaystyle\int_{p_1}^{1}\frac{K(1,\tilde{p})}{\bar{u}(\tilde{p})\,k-\sigma}\frac{\mathrm{d}h(\tilde{p})}{\mathrm{d}\tilde{p}}\,\mathrm{d}\tilde{p}}. \tag{29}$$

By substituting (28) and (29) into (19), we also obtain the analytic solution of $W(p)$ as

$$\begin{aligned}W(p)&=W_B\frac{\varepsilon k^2}{2}\left[2\lambda k\int_{p_1}^{1}G(p,\tilde{p})\right.\\&\times\int_{p_1}^{1}\frac{K(\tilde{p},\hat{p})}{\bar{u}(\hat{p})\,k-\sigma}\frac{\mathrm{d}h(\hat{p})}{\mathrm{d}\hat{p}}\,\mathrm{d}\hat{p}\,\mathrm{d}\tilde{p}\\&\left.-\int_{p_1}^{1}G(p,\tilde{p})\,h(\tilde{p})\,\mathrm{d}\tilde{p}\right]\\&\equiv W^{(\mathrm{d})}+W^{(\mathrm{h})}.\end{aligned} \tag{30}$$

All quantities appearing on the r.h.s. of (30) are known once the eigenvalue has been determined. It is tempting to interpret $W^{(\mathrm{d})}$ as the dynamically induced vertical velocity and $W^{(\mathrm{h})}$ as the diabatically induced vertical velocity since the former is directly associated with the vorticity advection term and the latter with the diabatic heating term in (16). However, such an interpretation has only limited validity because the dynamically induced part is also indirectly influenced by the heating through the effect of the latter on the streamfunction. Mathematically, the influence is manifested through the eigenvalue σ and W_B in the expression for $W^{(\mathrm{d})}$. Nevertheless, the interpretation above is still expected to be meaningful when the heating intensity is weak or moderate. In that event, $W^{(\mathrm{d})}$ would be primarily controlled by the dry dynamical process in the classic Eady mode. It is noted that (28), (29), and (30) constitute a complete general solution of the eigenfunction applicable for any heating profile.

2.4. *Analysis for a uniform heating profile*

We now apply the general dispersion relation (24) to a generic form of the heating profile. Let us consider a heating profile $h(p)$ which is equal to unity between two levels, p_{**} and p_*, and zero above p_{**} and below p_*. The expression for such a uniform heating profile is

$$\begin{aligned}h(p)&=H(p-p_{**})-H(p-p_*)\\&=\begin{cases}1 & \text{for } p_{**}<p<p_*,\\0 & \text{for } p<p_{**},\quad p>p_*,\end{cases}\end{aligned} \tag{31}$$

where H is the Heaviside unit step function. It follows that

$$\frac{\mathrm{d}h}{\mathrm{d}p}=\delta(p-p_{**})-\delta(p-p_*), \tag{32}$$

where δ is the Dirac delta function. With the use of (31) and (32), we can simplify the integral in (24) and obtain:

$$1+\frac{\varepsilon k^2}{2}\int_{p_{**}}^{p_*} G(p_B, p)\,dp$$

$$=r_{**}\int_{p_1}^{1} G(p_B, p)\,K(p, p_{**})\,dp$$

$$-r_*\int_{p_1}^{1} G(p_B, p)\,K(p, p_*)\,dp, \qquad (33)$$

where

$$r_{**}=\frac{\varepsilon\lambda k^3}{\bar{u}_{**}k-\sigma}, \qquad r_*=\frac{\varepsilon\lambda k^3}{\bar{u}_* k-\sigma}.$$

Eq. (33) is a generalization of eq. (23) in Mak (1982). It differs from the latter in that there is an additional integral on the l.h.s. of (33) and the effective heating intensity is equal to $\frac{1}{2}\varepsilon$. It will be seen from the actual computation that this additional integral has a great quantitative impact on the result when the heating intensity is moderate to large.

Eq. (33) is next used to determine the eigenvalues. Depending upon whether p_B is greater than or less than p_*, each of the three integrals in (33) must be applied as a sum of several integrals defined for different subintervals between p_1 and 1. Thus, we need to consider two distinct cases separately.

2.4.1. Case (i). Deep moist layer: $p_B < p_*$. The top of the surface moist layer is above the bottom of the heating layer (the cloud base) in this case. Then we have 4 subintervals separated sequentially by p_1, p_{**}, p_B, p_* and 1. It follows that (33) takes on the following explicit form.

$$1+\frac{\varepsilon k^2}{2}\left(\int_{p_{**}}^{p_B} G_2(p_B, p)\,dp+\int_{p_B}^{p_*} G_1(p_B, p)\,dp\right)$$

$$=r_{**}\left(\int_{p_1}^{p_{**}} G_2(p_B, p)\,K_1(p, p_{**})\,dp\right.$$

$$+\int_{p_{**}}^{p_B} G_2(p_B, p)\,K_2(p, p_{**})\,dp$$

$$\left.+\int_{p_B}^{1} G_1(p_B, p)\,K_2(p, p_{**})\,dp\right)$$

$$-r_*\left(\int_{p_1}^{p_B} G_2(p_B, p)\,K_1(p, p_*)\,dp\right.$$

$$+\int_{p_B}^{p_*} G_1(p_B, p)\,K_1(p, p_*)\,dp$$

$$\left.+\int_{p_*}^{1} G_1(p_B, p)\,K_2(p, p_*)\,dp\right). \qquad (34)$$

Since the two Green's functions $G_j(p, \tilde{p})$ and $K_j(p, \tilde{p})$, $j=1, 2$ are made up of linear combinations of exponential functions, the integration of each integral in (34) can be analytically carried out. After doing that and some algebraic rearrangement, it can be shown that (34) takes on the form of a fourth order polynomial in σ. We may write the resulting equation symbolically as:

$$A_4\sigma^4+A_3\sigma^3+A_2\sigma^2+A_1\sigma+A_0=0, \qquad (35)$$

where each of the coefficients is a very lengthy expression of the model parameters, namely

$$A_j=A_j(S, \lambda, k, \varepsilon, p_1, p_{**}, p_B, p_*),$$
$$j=0, 1, 2, 3, 4.$$

For conciseness, the explicit expressions for A_j are not presented.

2.4.2. Case (ii). Shallow moist layer: $p_* < p_B$. The top of the surface moist layer is below the bottom of the heating layer in this case. Then the subintervals are sequentially separated by p_1, p_{**}, p_*, p_B, and 1. Eq. (33) then takes on the following explicit form.

$$1+\frac{\varepsilon k^2}{2}\int_{p_{**}}^{p_*} G_2(p_B, p)\,dp$$

$$=r_{**}\left(\int_{p_1}^{p_{**}} G_2(p_B, p)\,K_1(p, p_{**})\,dp\right.$$

$$+\int_{p_{**}}^{p_B} G_2(p_B, p)\,K_2(p, p_{**})\,dp$$

$$\left.+\int_{p_B}^{1} G_1(p_B, p)\,K_2(p, p_{**})\,dp\right)$$

$$-r_*\left(\int_{p_1}^{p_*} G_2(p_B, p)\,K_1(p, p_*)\,dp\right.$$

$$+\int_{p_*}^{p_B} G_2(p_B, p)\, K_2(p, p_*)\, dp + \int_{p_B}^{1} G_1(p_B, p)\, K_2(p, p_*)\, dp\Big). \quad (36)$$

Eqs. (34) and (36) are generalization of eq. (24) in Mak (1982). Eq. (36) can be also written explicitly as a fourth order polynomial in σ. The coefficients are, of course, different from those for case (i). We can, therefore, readily determine the four eigenvalues for any parameter setting.

The corresponding eigenfunction of Ψ can be easily obtained from (28) with the use of (32). It is:

- *Above cloud top:* $p_1 \leqslant p \leqslant p_{**}$

$$\Psi = \left[\frac{(\sigma-\bar{u}_{**}k)\,\theta_* - (\sigma-\bar{u}_*k)\,\theta_{**}}{(\sigma-\bar{u}_{**}k)\,\gamma_* - (\sigma-\bar{u}_*k)\,\gamma_{**}}\right]\frac{\gamma}{\theta_1}. \quad (37a)$$

Here the notation is $\theta_* = \theta(p_*)$, $\theta_1 = \theta(1)$, $\theta_{**} = \theta(p_{**})$, etc. The expressions for γ and θ are given in (23).

- *Within cloud layer:* $p_{**} \leqslant p \leqslant p_*$

$$\Psi = \left[\frac{(\sigma-\bar{u}_{**}k)\,\theta_*\gamma - (\sigma-\bar{u}_*k)\,\gamma_{**}\theta}{(\sigma-\bar{u}_{**}k)\,\gamma_* - (\sigma-\bar{u}_*k)\,\gamma_{**}}\right]\frac{1}{\theta_1}. \quad (37b)$$

- *Below cloud base:* $p_* \leqslant p \leqslant 1$

$$\Psi = \frac{\theta}{\theta_1}. \quad (37c)$$

It is easy to verify that this solution of Ψ for a normal mode has zero potential vorticity everywhere except at p_{**}, p_*, and the boundaries of the domain, (p_1 and 1) as it should be.

We next apply (32) to the general expression (29) for the vertical velocity at p_B in this case of a uniform heating layer and obtain

$$W_B = \frac{i2b(\sigma-\bar{u}_{**}k)(\sigma-\bar{u}_*k)}{\varepsilon\theta_1[(\sigma-\bar{u}_{**}k)\,\gamma_* - (\sigma-\bar{u}_*k)\,\gamma_{**}]}. \quad (38)$$

To obtain the eigenfunction of $W^{(d)}$, $W^{(h)}$, and hence W, at all levels, we substitute (31) and (32) into (30) and perform the integration analytically. The result is:

- *Above cloud top:* $p_1 \leqslant p \leqslant p_{**}$

$$W^{(d)} = W_B\{J_{11}(p)\,\eta(p) + [J_{21}(p) + J_{22}(p_{**}) + J_{23}(p_*)]\,\xi(p)\},$$
$$W^{(h)} = W_B\, g_1\, \xi(p). \quad (39a)$$

- *Within cloud layer:* $p_{**} \leqslant p \leqslant p_*$

$$W^{(d)} = W_B\{[J_{11}(p_{**}) + J_{12}(p)]\,\eta(p) + [J_{22}(p) + J_{23}(p_*)]\,\xi(p)\},$$
$$W^{(h)} = W_B[g_2(p)\,\eta(p) + g_3(p)\,\xi(p)]. \quad (39b)$$

- *Below cloud base:* $p_* \leqslant p \leqslant 1$

$$W^{(d)} = W_B\{[J_{11}(p_{**}) + J_{12}(p_*) + J_{13}(p)]\,\eta(p) + J_{23}(p)\,\xi(p)\},$$
$$W^{(h)} = W_B\, g_4 \eta(p), \quad (39c)$$

where

$$J_{11}(p) = \alpha_1 \int_{p_1}^{p} \xi\gamma\, dp,$$

$$J_{12}(p) = \alpha_2 \int_{p_{**}}^{p} \xi\theta\, dp - \alpha_3 \int_{p_{**}}^{p} \xi\gamma\, dp,$$

$$J_{13}(p) = \alpha_4 \int_{p_*}^{p} \xi\theta\, dp,$$

$$J_{21}(p) = \alpha_1 \int_{p}^{p_{**}} \eta\gamma\, dp,$$

$$J_{22}(p) = \alpha_2 \int_{p}^{p_*} \eta\theta\, dp - \alpha_3 \int_{p}^{p_*} \eta\gamma\, dp,$$

$$J_{23}(p) = \alpha_4 \int_{p}^{1} \eta\theta\, dp,$$

$$g_1 = -\frac{\varepsilon k^2}{2a}\int_{p_{**}}^{p_*} \eta\, dp,$$

$$g_2 = -\frac{\varepsilon k^2}{2a}\int_{p_{**}}^{p} \xi\, dp,$$

$$g_3 = -\frac{\varepsilon k^2}{2a}\int_{p}^{p_*} \eta\, dp,$$

$$g_4 = -\frac{\varepsilon k^2}{2a}\int_{p_{**}}^{p_*} \xi\, dp,$$

$$\alpha_1 = \frac{\lambda k^3 \varepsilon}{ab}\left(\frac{\theta_{**}}{\bar{u}_{**}k-\sigma} - \frac{\theta_{*}}{\bar{u}_{*}k-\sigma}\right),$$

$$\alpha_2 = \frac{\lambda k^3 \varepsilon}{ab}\frac{\gamma_{**}}{\bar{u}_{**}k-\sigma},$$

$$\alpha_3 = \frac{\lambda k^3 \varepsilon}{ab}\frac{\theta_{*}}{\bar{u}_{*}k-\sigma},$$

$$\alpha_4 = \frac{\lambda k^3 \varepsilon}{ab}\left(\frac{\gamma_{**}}{\bar{u}_{**}k-\sigma} - \frac{\gamma_{*}}{\bar{u}_{*}k-\sigma}\right).$$

The integrals in the J's and g's can be readily worked out and are not presented for conciseness. Equations (37), (38), and (39) constitute a complete solution of the eigenfunction in explicit form for the case of a uniform heating layer. It should be noted that while Ψ is continuous at p_{**} and p_{*}, its vertical derivative and, hence, the temperature perturbation is discontinuous there. Both W and its derivative are, however, continuous at the top and bottom of the heating layer.

3. Result

3.1. General comment

The dispersion relation (35) indicates that there can be only four normal modes in this model setting. It is pertinent to ask at the outset: what is the physical basis for this simple mathematical consequence? The answer to this question is clearest to see from the potential vorticity (PV) point of view. Recall that the flow in the classical Eady model has zero PV throughout the interior. The meridional gradient of the basic temperature at the boundaries is equivalent to the presence of a sheet of basic PV with a finite meridional gradient immediately adjacent to each of the boundaries. Such a basic potential vorticity field can therefore support one wave mode at each boundary. Those two wave modes are often referred to as edge waves. The vertical extent of these waves is larger for a longer horizontal wavelength. If the wavelength is sufficiently short, the two edge waves could not significantly interact with one another. They would remain virtually uncoupled and would be neutral. When the wavelength exceeds a certain threshold value, the vertical extent of each edge wave would reach the other boundary and they could reinforce one another through the potential vorticity advection with a certain relative phase. This leads to a structure with a tilt leaning against the basic shear. Such a structure also enables them to intensify by extracting energy from the basic thermal field. This is the reason for the existence of a shortwave cutoff of the baroclinic instability from the potential vorticity point of view (Bretherton, 1966). The dynamical nature of baroclinic instability in the Charney model can be similarly interpreted (Robinson, 1989). The growth rate has a maximum value for a certain intermediate wavelength where there is an optimal reinforcement between the two waves. Now, a finite PV anomaly would be generated by the heating wherever there is a vertical gradient in the condensational heating rate. The normal mode would then result from the interactions among the PV anomalies at the top and bottom of the domain as well as those at all levels in the heating layer with the use of a general heating profile. That is why the dispersion relation can be readily written in terms of a double integral for the case of a general heating profile, eq. (24). For the special case of a top-hat heating profile, the heating rate changes with height only at the top and bottom of the layer. Therefore, two additional wave modes can be supported. This is the physical basis of the existence of four eigenvalues resulting in a quartic equation as the dispersion relation. The complication concerning the character of the four eigenmodes then arises from the various possible interactions among the different PV anomalies. The self-induced heating would have qualitatively new impacts on the instability properties when the two interior singular levels associated with the heating play a major role as the two rigid boundaries of the domain associated with the basic baroclinicity.

3.2. Instability properties of the normal modes (eigenvalue)

The eigenvalues are computed by solving the appropriate version of the quartic eq. (35) for the case of either a deep or a shallow surface moist layer. A meaningful set of dimensional values for the parameters is:

$p_1 = 150$ mb, $p_{**} = 400$ mb, $p_{*} = 900$ mb,

$p_b = 900$ mb, $p_{00} = 1000$ mb,

$\lambda = 30/(p_{00} - p_1)$ ms^{-1} mb^{-1},

$S = 0.04$ m^2 s^{-2} mb^{-2},

$f = 10^{-4}$ s^{-1}, $\varepsilon = 1$ K mb^{-1}.

Using $U = 10\ \mathrm{ms}^{-1}$ and $L = 10^6$ m as the velocity and length scales, the values of the nondimensional parameters (again after dropping the prime) would be:

$$\lambda = 3.5, \qquad S = 4.0, \qquad \varepsilon = 30,$$

$$p_1 = 0.15, \qquad p_{**} = 0.4,$$

$$p_* = 0.9, \qquad p_b = 0.9.$$

We will refer to this parametric conditions as the reference case. One nondimensional time unit would correspond to $10^5\ \mathrm{s} \approx 1$ day.

It may be more instructive to assess the heating intensity parameter ε in terms of the heating rate Q in K/day. Recall that the heating rate in this model analysis depends on the product of $\frac{1}{2}\varepsilon$ and ω_B (see eq. (14)). The scale of ω, denoted as $\hat{W}$, may be related to the scale of the other variables in accordance with the quasi-geostrophic scaling argument, viz.

$$\frac{\hat{W}}{p_{00}} \sim \mathrm{div} \sim \frac{U}{L}\mathrm{Ro}$$

$$\Rightarrow \hat{W} \sim 1 \times 10^{-3}\ \mathrm{mb\ s}^{-1};$$

Ro is the Rossby number.

Since ω_B is at a level quite close to the surface boundary, one would expect its magnitude to be somewhat smaller than the scale $\hat{W}$ itself by several folds. On the other hand, $\hat{W}$ may be increased by several folds in the presence of condensational heating because the horizontal scale L is expected to be reduced and the velocity scale increased as we will see from the analysis later. In light of these additional considerations, it seems to be consistent to use $\omega_B \sim 2\hat{W}$ as a rough estimate when the effect of heating is strong. If we use $\omega_B = 2 \times 10^{-3}\ \mathrm{mb\ s}^{-1}$, the heating rate corresponding to $\varepsilon_{\mathrm{dim}} = 1\ \mathrm{K\ mb}^{-1}$ in this model would be $Q \sim \frac{1}{2}\varepsilon\omega_B \sim 80$ K/day. The model results may then be relevant for $\varepsilon_{\mathrm{dim}}$ up to $2\ \mathrm{K\ mb}^{-1}$. We will see that all major effects on the moist baroclinic instability are found for $\varepsilon < 1\ \mathrm{K\ mb}^{-1}$. Furthermore, we will see from the calculation that the effect of heating does not monotonically vary with ε, but is actually strongest for $\varepsilon \sim 1\ \mathrm{K\ mb}^{-1}$. Hence for even larger ε, we may actually use a smaller ω_B to estimate Q which would then not be as large as it might seem. The validity of quasi-geostrophic argument in conjunction with a strong condensational heating is clearly stretched to the limit in a modelling study of this type. But as long as the chosen model parametric values are geophysically realizable, it would serve little to take too literal an interpretation of them in the course of inferring the moist dynamics from the results of this highly idealized model.

We only have indirect and crude information about Q and ω_B in cyclones strongly influenced by condensation heating. According to the simulation of Kuo et al. (1991), most of the condensational heating in the QE-II storm occurs between 350 and 950 mb with largest values in the layer between 550 mb and 850 mb, and the maximum heating rate reaches about 550 K/day albeit in a relatively narrow region (see their Fig. 13a). The heating region in that model is about 250 km wide and the average heating rate over that region is nevertheless in excess of 100 K/day. Estimate of the vertical velocity in an intensifying cyclone over an oceanic region is rather imprecise because of sparcity of data. Gyakum (1983) kinematically computes the horizontal divergence at the surface and 250-mb from the wind data, linearly interpolates the divergence values at the levels in between, applies a correction and then evaluates the corresponding ω structure. Such computation reveals that as the QE-II storm is at its accelerated stage of development (1200 GMT on 9 September 1978), the ω at 900 mb taken to be ω_B is $5 \times 10^{-3}\ \mathrm{mb\ s}^{-1}$ (see his Fig. 19a). Whitaker et al. (1988) use a model simulation to generate the ω field in another explosive cyclone, known as the President's Day storm which rapidly intensifies at 0300 UTC on 19 February 1979. Their model value of ω at 900 mb immediately prior to rapid cyclogenesis is $1 \times 10^{-3}\ \mathrm{mb\ s}^{-1}$ (see their Fig. 8c for 1200 UTC 18 February). It increases to about $10 \times 10^{-3}\ \mathrm{mb\ s}^{-1}$ at the mature stage by 1200 UTC 19 February (see their Fig. 6c). The independent estimates of ω_B by Gyakum and Whitaker et al., for two different storms are comparable and are compatible with our previous estimate of ω_B on the basis of crude scaling argument.

A wide range of the heating intensity $0.01 < \varepsilon < 60$ is examined to ascertain the sensitivity to this parameter. In each parameter setting, the wavelength of the normal mode is scanned over two orders of magnitude with a small increment in

order to make a complete quantitative determination of the instability properties. The computed eigenvalue for each parametric setting is plotted as a point in the following diagrams. We will also examine the cases where $p_b \neq p_*$.

Let us begin by examining the effects of the heating when the heating intensity is weak to moderate. Fig. 1 shows that the variation of the growth rate σ_i of the four modes with wavelength for different Q from 0.02 to 48 K/day. A short-wave cutoff is well defined in each case. For wavelengths longer than the cutoff wavelength, there exists one amplifying mode and one decaying mode. Two neutral modes supplement the pair of complex modes. When the heating is very small ($Q = 0.02$ K/day), the classic Eady result is recovered as one would expect. The maximum growth rate in this case is about $0.52 \times 10^{-5}\ s^{-1}$ for a wavelength of 6700 km, amounting to an e-folding time of 2 days. The phase velocity of the unstable modes has been verified to be equal to $c = \sigma_\tau / k = 1.5$, the non-dimensional basic mean flow at the mid-level of the domain.

The dramatic impact of the condensational heating is more clearly depicted in Fig. 2 showing the variation of the maximum growth rate of

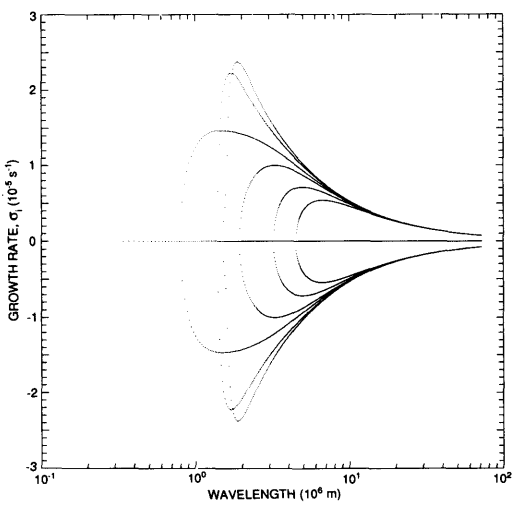

Fig. 1. Variations of the growth rate σ_i of the four eigenmodes with wavelength for six nondimensional values of the heating intensity, $\varepsilon = 0.01$, 8, 13, 15, 17, 18 ($\varepsilon = 30 \leftrightarrow Q = 80$ K/day). Inner most curve is for the smallest value of ε. Other parameters have values of the reference case. Two modes are neutral and have $\sigma_i = 0$. Each dot is a data point.

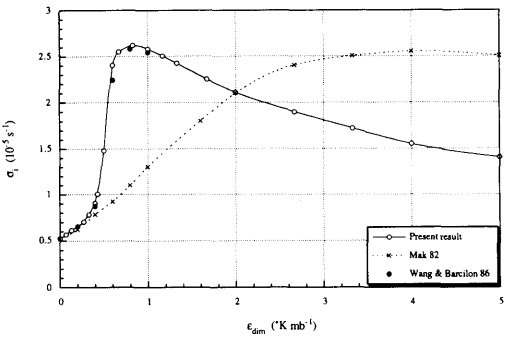

Fig. 2. Variation of the maximum growth rate of the moist Eady mode with the dimensional heating parameter. A comparison of the counterpart results in Mak (1982) and Wang and Barcilon (1986).

the moist Eady mode with the heating intensity parameter ε. It reveals a highly nonlinear dependence. The maximum growth rate first gradually increases with ε and then sharply increases in the range of $0.4 < \varepsilon_{dim} < 0.7$ K mb^{-1} corresponding to $32 < Q < 56$ K/day. It increases by a factor of 5 from $0.52 \times 10^{-5}\ s^{-1}$ to $2.6 \times 10^{-5}\ s^{-1}$ when Q is increased to 60 K/day. The trend is then reversed with the growth rate decreasing gradually with further increase in Q. The result is also compared with the counterpart results given in Mak (1982) and in Wang and Barcilon (1986) in Fig. 2. It should be noted that the value of ε_{dim} in those two other analyses should be doubled for comparison because the necessary factor of $\frac{1}{2}$ as shown in eq. (14) was not included in their calculation. Although my earlier growth rate curve (Mak, 1982; taken from his Fig. 3) is qualitatively similar to that of the present analysis, the feature of highly nonlinear dependence is missing and the value of ε_{dim} for the largest possible growth rate is changed from 4.0 K mb^{-1} in the last analysis to 0.8 K mb^{-1} in this analysis. The reason for this discrepancy is that the approximation introduced in Mak (1982) suppresses the direct feedback effect of the heating on the vertical velocity field itself. The strong effect of the heating would therefore not be manifested until a much larger Q is used. That assumption, which is shown to be unnecessary in this analysis, is only justifiable for a weak heating. The current results closely agree with the counterpart results in Wang and Barcilon (for $\varepsilon_{dim} = 1$ K mb^{-1}; taken from their Table 5). Their method of analysis is equivalent to but quite

different from the one used here. One cannot infer by inspection from their dispersion relation (eq. (4.7)) that there actually exist only four eigenvalues for the case of a uniform heating profile. Nor did they extensively examine the instability properties for this generic case. Their discussion primarily focussed on an evaluation of the growth rate and phase speed of the unstable waves for three other heating profiles.

The highly nonlinear variation of the wavelength of the most unstable moist Eady mode, L_{max}, with the heating intensity parameter ε is equally dramatic. Fig. 3 shows that L_{max} first sharply decreases by a factor of 4.7 from 6700 km to 1400 km when the heating rate Q increases to 48 K/day (ε_{dim} increases to 0.6 K mb^{-1}). This pronounced reduction of scale is consistent with the observation that the storms that are greatly influenced by condensational heating tend to have a tighter inner structure. It warrants to emphasize that this significant change of length scale is not a direct consequence of an explicitly prescribed reduction of the static stability as reported in some studies (e.g., Nakamura, 1988). It is rather an internal dynamical effect of a self-induced condensational heating. The same static stability is used in this series of computation for different heating intensity. This trend of decreasing L_{max} is reversed for $\varepsilon_{dim} > 0.6$ K mb^{-1}. The comparison of my previous result (dash in Fig. 3) again reveals that it is greatly distorted although the general feature of the dash curve is similar to the present one. The smallest possible value of L_{max} in Mak (1982) reaches a minimum of 2300 km for $\varepsilon_{dim} = 2.5$ K mb^{-1} instead of 1400 km for $\varepsilon_{dim} = 0.6$ K mb^{-1} obtained in this analysis. This is also a major manifestation of the consequence of the approximation used in that study. The limited results (solid circles) of Wang and Barcilon (1986) again agree closely with the present results. There is a corresponding change in the trend about the variation of the shortwave cutoff with the heating intensity.

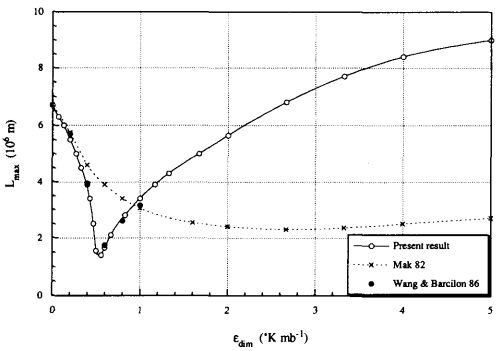

Fig. 3. Variation of the wavelength of the most unstable moist Eady mode with the dimensional heating parameter. A comparison of the counterpart results in Mak (1982) and Wang and Barcilon (1986).

The reversal of the trends discussed above was reported in the several previous studies of moist baroclinic instability, but no clear physical interpretations were given (e.g., Bannon, 1986). Now the potential vorticity point of view permits a simple dynamical interpretation of the trends in this generic setting of heating. They may be viewed as a natural consequence of the interference of the interaction between the two PV anomalies at the model surface and model tropopause by the presence of the two additional PV anomalies at the top and bottom levels of the heating layer associated with a strong heating. A sufficiently strong interference distorts the structure of the moist Eady mode so much that its overall efficiency in extracting energy from the basic state is reduced.

We have seen pronounced impacts of a self-induced condensational heating on the growth rate and length scale. The theoretical model results are fairly compatible with the limited observational evidence. The class of unstable modes discussed above is clearly a moist unstable Eady mode. Energetically, the condensational heating gives rise to an additional source of potential energy for the instability process. Dynamically, the self-induced heating layer facilitates the two edge-waves to interact more efficiently and thereby to phase-lock themselves to a more favorable structure.

A new result, which has not been reported in the previous analyses, begins to appear when the non-dimensional heating intensity parameter exceeds about 20, corresponding to $Q = 53$ K/day. It is manifested as the existence of a new branch of unstable modes with wavelengths shorter than the shortwave cutoff of the modified Eady mode. The range of wavelengths of this new branch becomes wider for a larger heating intensity. Furthermore, a second new branch of unstable modes with even shorter wavelengths also emerges when the heating

rate reaches $Q = 70$ K/day. It too only exists for a certain limited range of wavelength which also becomes wider for a larger heating intensity. The two panels of Fig. 4 for $Q = 53$ and 160 K/day serve to clearly reveal the various interesting features of the new unstable modes. These features in Fig. 4b are robust in that the main features vary relatively little over a substantial range of ε. We will defer the discussion about their physical nature until after we have presented the structure of these modes in the next subsection.

The results of the frequency of the eigenmodes are presented in Fig. 5 as a function of the wavelength for two values of heating intensity, $Q = 26$ and 160 K/day. All other parameters have the values of the reference case. For a weak heating, only two of the modes bifurcate into a pair of modified Eady unstable/stable modes at the shortwave cutoff (Fig. 5a). The corresponding phase velocity of the modified unstable Eady mode varies from 1.7 to 1.5 and is thus slightly higher than that of the dry Eady mode. This effect is consistent with the finding in the simulation study of Kuo et al. (1991). It signifies a stronger influence of the PV anomalies at the top of the heating layer.

As in the growth rate curve, there are two additional bifurcations in the frequency curves in the shorter range of wavelength when the heating is sufficiently large (Fig. 5b). One branch of modes has a relatively high frequency, as exemplified by the mode with a wavelength of 2×10^6 m and a frequency of $7 \times 10^{-5}\,s^{-1}$. The corresponding phase velocity is about $c = \sigma_r/k = 2.3$. This value is equal to the basic flow at a steering level close to the mid-level between the model tropopause and the top of the heating layer $(\frac{1}{2}(\bar{u}(p_1) + \bar{u}(p_{**})) = 2.2)$. The other branch of modes emerges when the heating rate Q exceeds 70 K/day. An example of this branch of unstable modes is the mode with a wavelength of 5×10^5 m and a frequency of $2 \times 10^{-5}\,s^{-1}$. The corresponding phase velocity of this mode is only about 0.18. This value is equal to the basic flow at a steering level close to the mid-level between the model surface and the bottom of the heating layer $(\frac{1}{2}\bar{u}(p_*) = 0.175)$. On the basis of these quantitative results, we may anticipate that the first additional branch of unstable modes is an upper tropospheric wave, whereas the second additional branch of unstable modes is a lower tropospheric wave. This will be verified on the basis of their structures. Each of these unstable modes has a shortwave cutoff which is mainly related to the thickness between the domain boundary and the relevant internal boundary. The lower mode has a shorter wavelength than the upper mode because the distance between the cloud base and the model surface happens to be shorter than that between the cloud top and the model tropopause. There should be always a shortwave cutoff for the mechanism of Baroclinic-CISK simply because of the nature of quasi-geostrophic baroclinic instability. This anticipation is indeed borne out by the details of the computational results.

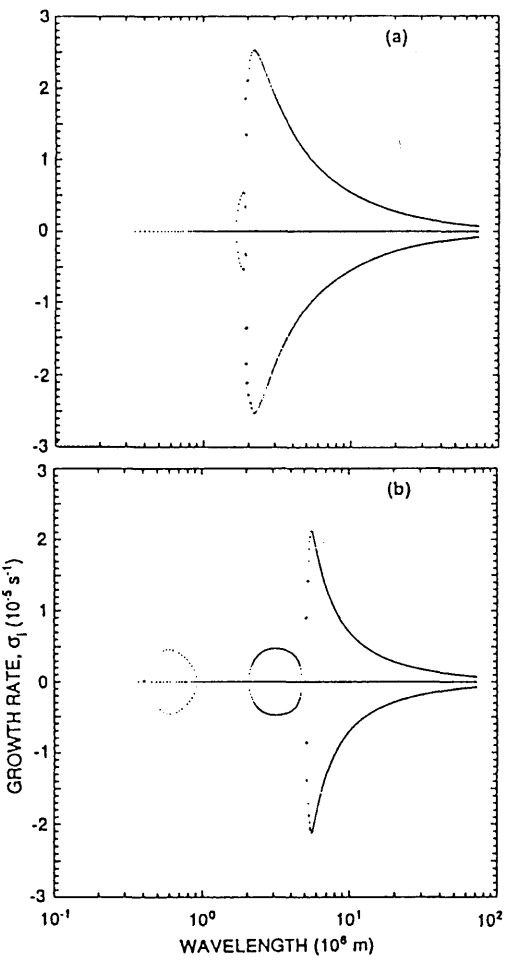

Fig. 4. Variations of the growth rate σ_i of the four eigenmodes with wavelength for the heating intensity (a) $\varepsilon = 20$ and (b) $\varepsilon = 60$. ($\varepsilon = 30 \leftrightarrow Q = 80$ K/day). Other parameters have values of the reference case.

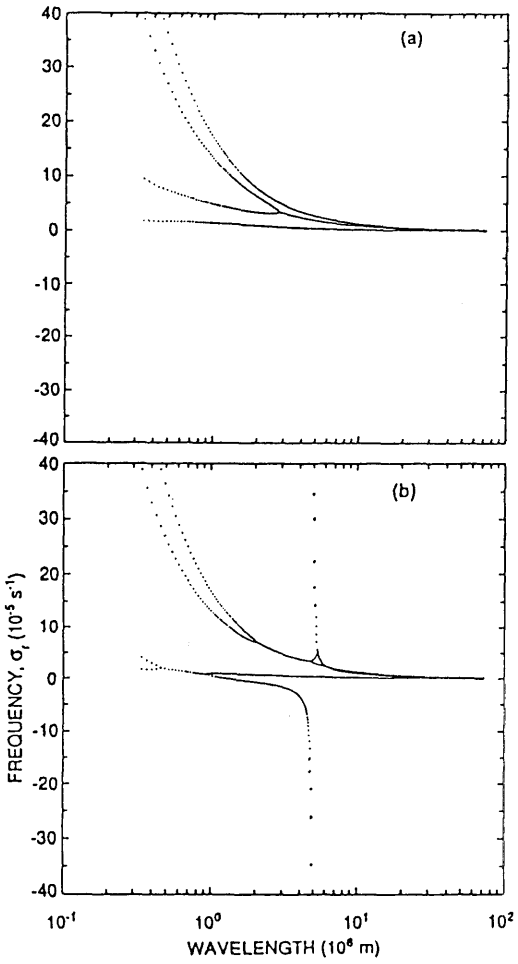

Fig. 5. Variations of the frequency σ_r of the four eigenmodes with wavelength for the heating intensity (a) $\varepsilon = 10$ and (b) $\varepsilon = 60$. ($\varepsilon = 30 \leftrightarrow Q = 80$ K/day). Other parameters have values of the reference case.

3.3. *Structure of the unstable modes (eigenfunction)*

The physical nature of the unstable modes discussed above is indeed quite evident in their structural characteristics. The eigenfunction of the streamfunction is computed with eqs. (37a, b, c). Fig. 6 shows the structure of the streamfunction of one representative unstable mode from each of the three distinctly different groups of unstable modes for $\varepsilon = 60$. The wavelengths of these three modes are distinctly different. Fig. 6a shows the streamfunction of the unstable moist Eady mode with a wavelength of 6000 km. Its tilt is larger than that of a dry Eady mode, giving rise to a larger growth rate. Fig. 6b shows the result for an unstable mode with a wavelength of 3000 km. This structure is concentrated between the model tropopause and the top of the heating layer. This mode arises from the two edge-waves associated with the top of the heating layer and the model tropopause. The vertical structure has a westward tilt. It is conjectured that some of the common short wave disturbances in the upper troposphere could be identifiable with this mode. Fig. 6c shows the counterpart for an unstable mode with a wavelength equal to 600 km. In contrast, it is concentrated in the layer between the surface and the bottom of the heating layer.

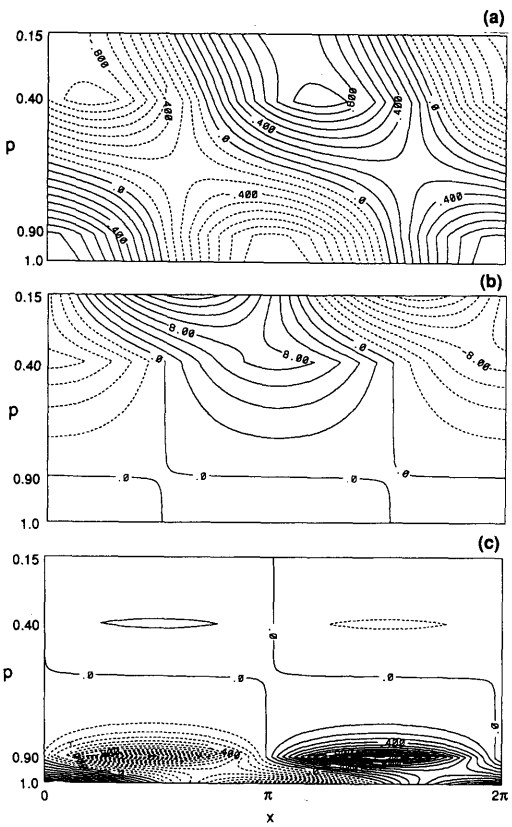

Fig. 6. Structure of the nondimensional streamfunction of a representative mode from each distinct group of unstable modes for the reference case parametric condition and $\varepsilon = 60$. (a) A moist Eady mode with a wavelength of 6000 km. (b) A diabatically induced upper mode with a wavelength of 3000 km. (c) A diabatically induced lower mode with a wavelength of 600 km.

It is reminiscent of some of the shallow storms encountered occassionally with substantial precipitation such as the polar lows. It also has a westward tilt of phase confined in that layer. The two modes shown in Fig. 6b and c are referred to as the upper and lower heating-induced modes. It should be emphasized that although the condensational heating is an indispensable factor for the existence of these two unstable modes, the basic shear is equally essential. The absence of a baroclinic shear would mean the absence of the sheets of potential vorticity at the top and bottom of the domain. The physical nature of these modes from the PV perspective is quite clear. When the heating is strong, the PV anomaly at the model tropopause mainly interacts with that at the top of the heating layer, and PV anomaly at the model surface mainly interacts with that at the bottom of the heating layer. The optimal wavelength of these additional branches of unstable modes depends largely upon the thickness of the two corresponding sublayers.

It is pertinent to recall that each eigenfunction of the streamfunction has been arbitrarily normalized to unity at the bottom boundary ($p = 1$), namely $\Psi(1) = 1$. The modified Eady mode (Fig. 7b) and the lower mode (Fig. 7c) have their maximum value of ψ at the bottom boundary, $p = 1$. In contrast, the upper mode (Fig. 7b) has its minimum value of ψ at $p = 1$. Consequently, the maximum value of ψ of the upper mode is much larger than unity (~ 17) leading to correspondingly large values of ω. Therefore, it is meaningless to compare the absolute value of all eigenfunctions normalized to unity at one arbitrarily chosen level. They however have unique and meaningful structures.

Eqs. (39a, b, c) are next used to compute the vertical structure of the dynamical part ($W^{(d)}$) and the diabatically induced part ($W^{(h)}$) of the vertical velocity of the three modes under consideration. Fig. 7 shows their amplitude and phase angle as well as those of $W = W^{(d)} + W^{(h)}$ for the modified Eady mode with a wavelength of 6000 km. The phase of $W^{(d)}$ has a westward tilt of about 120° (dot curve in Fig. 7b), whereas $W^{(h)}$ has no vertical tilt by definition (dash curve in Fig. 7b). The total vertical velocity of this mode has a net westward tilt of $\sim 60°$. Its magnitude is stronger than those of the two individual components. The heating is already so large in this case ($Q =$ 80 K/day) that the heating is the dominant driving mechanism of the vertical velocity as evidenced by a much larger amplitude in $W^{(h)}$ than in $W^{(d)}$ (dash versus dot curves in Fig. 7a). This result is consistent with the finding in the numerical simulation study of Kuo et al. (1991). Nevertheless, this mode is qualitatively similar to a dry Eady mode and has been reported in the previously cited studies.

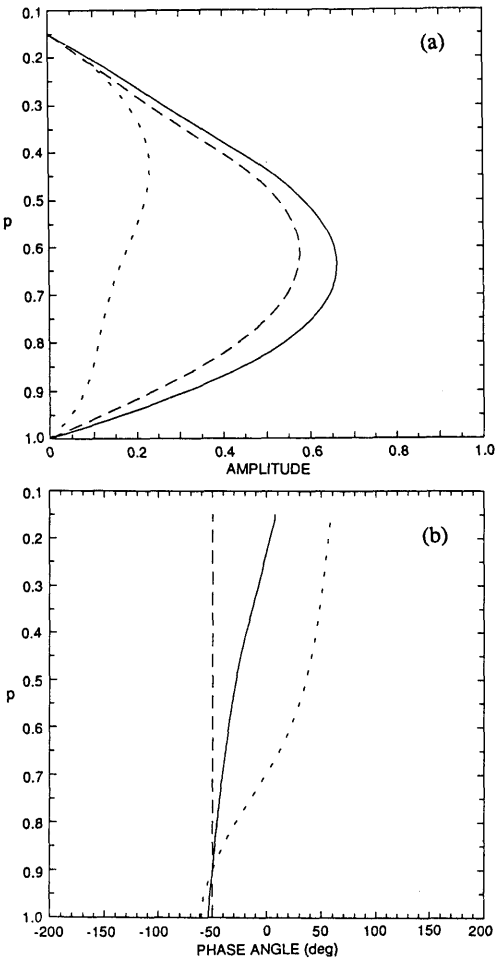

Fig. 7. Vertical structure of the corresponding non-dimensional vertical velocity of the moist Eady mode with a wavelength of 6000 km. (a) Amplitude of W (solid), $W^{(d)}$ (dot) and $W^{(h)}$ (dash). (b) Phase angle of the corresponding three quantities; $W = W^{(d)} + W^{(h)}$.

Fig. 8 shows the counterpart result for the most unstable mode of the first new subset of modes. It

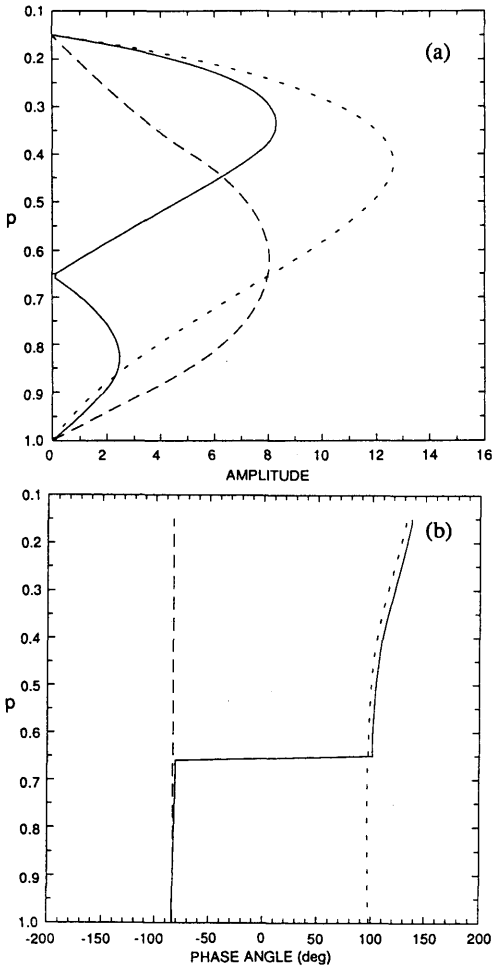

Fig. 8. Vertical structure of the corresponding non-dimensional vertical velocity of the diabatically induced upper mode with a wavelength of 3000 km. (a) Amplitude of W (solid), $W^{(d)}$ (dot) and $W^{(h)}$ (dash). (b) Phase angle of the corresponding three quantities; $W = W^{(d)} + W^{(h)}$.

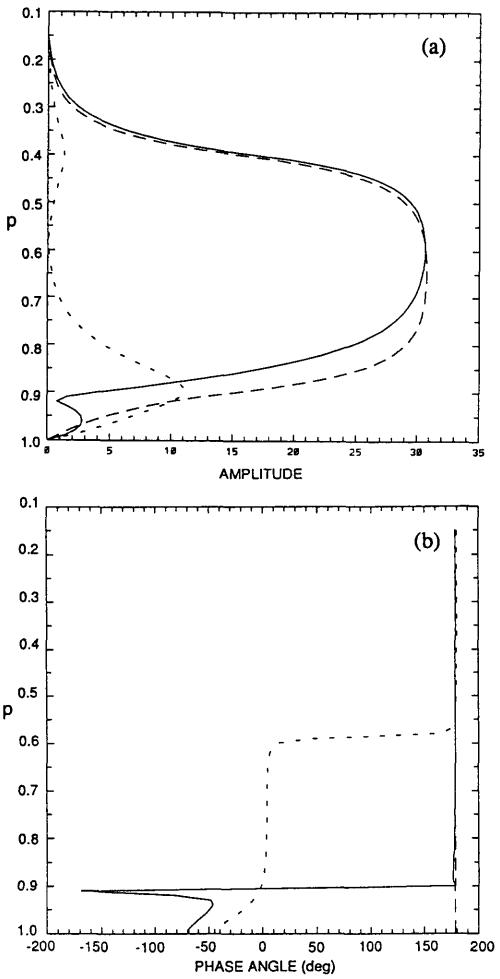

Fig. 9. Vertical structure of the corresponding non-dimensional vertical velocity of the diabatically induced lower mode with a wavelength of 600 km. (a) Amplitude of W (solid), $W^{(d)}$ (dot) and $W^{(h)}$ (dash). (b) Phase angle of the corresponding 3 quantities; $W = W^{(d)} + W^{(h)}$.

has a wavelength of 3000 km. The vertical velocity field is strongest near the top of the heating layer. A secondary maximum is found at $p = 0.85$. While the amplitude of $W^{(d)}$ and $W^{(h)}$ are comparable below about $p = 0.65$, their phase angles differ by nearly 180°, resulting in a much weaker total W. Above $p = 0.65$, $W^{(d)}$ is progressively stronger than $W^{(h)}$. Hence, the total W is close to that of $W^{(d)}$. This mode may then be referred to as the upper mode.

Fig. 9 shows the counterpart result for the most unstable mode of the second new branch of modes. It has a much shorter wavelength of 600 km. The structure of the total vertical velocity field in this mode is mostly attributable to $W^{(h)}$ except near the bottom surface. Note that although the stream-function is mostly confined below the heating layer (Fig. 6c), the vertical velocity field extends to most of the vertical domain. There may be then substantial cloudiness and precipitation associated with

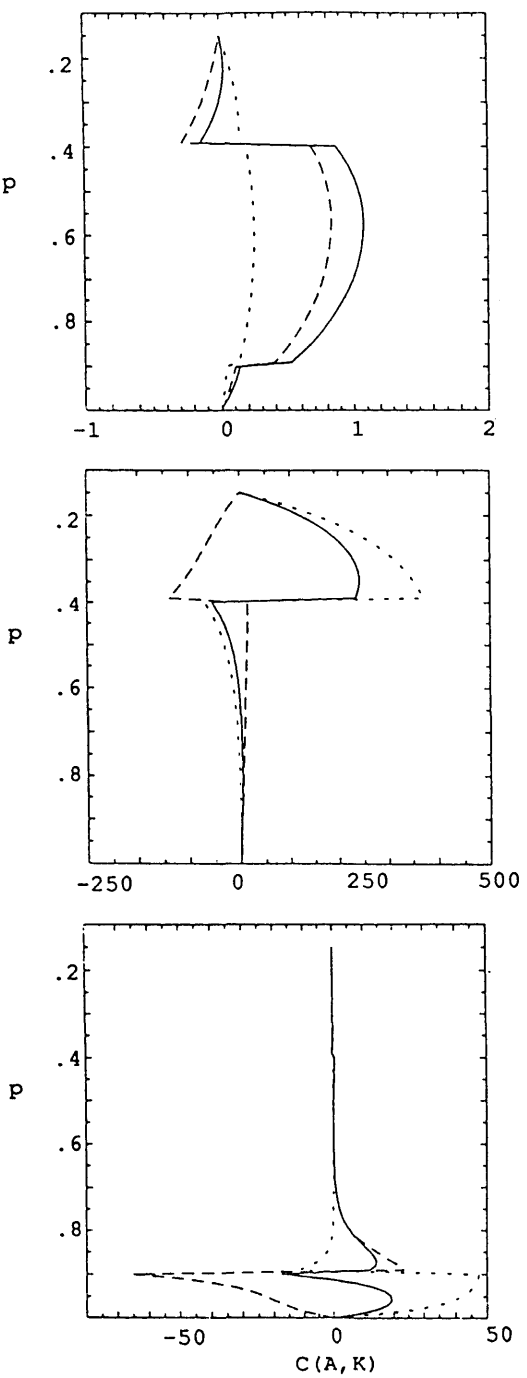

Fig. 10. Vertical distribution of the corresponding non-dimensional conversion rate from available potential energy to kinetic energy, $C(A, K)$, for the 3 normal modes with a wavelength (a) 6000 km, (b) 3000 km and (c) 600 km. The solid curve is for the total conversion rate; the dot curve is for the conversion rate associated with $W^{(d)}$; the dash curve is for the conversion rate associated with $W^{(h)}$.

such a mode. Below $p=0.9$, $W^{(d)}$ and $W^{(h)}$ are greatly out of phase with comparable amplitude. This results in a small total W near the surface. This mode was also not reported in the other studies. In light of the various attributes of this unstable mode, it could be identifiable with the relatively small and shallow storms simulated by Grønås et al. (1992) and Kristjansson (1990).

3.4. Energetic

The distinct physical identity of the unstable modes can be also seen from the characteristics of their energetic. It suffices to examine the conversion rate of kinetic energy from the potential energy. The potential energy partly comes from the basic thermal state and partly from the heating. It may be computed as

$$\begin{aligned} C(A, K) &= \int_0^{2\pi} \int_{p_1}^1 \omega \frac{\partial \psi}{\partial p} \, dx \, dp \\ &= \frac{1}{2} \int_{p_1}^1 \left(\mathrm{Re} \left\{ W^{(d)} \frac{d\Psi^*}{dp} \right\} \right. \\ &\quad \left. + \mathrm{Re} \left\{ W^{(h)} \frac{d\Psi^*}{dp} \right\} \right) dp, \end{aligned} \tag{40}$$

where the asterisk denotes the complex conjugate. Fig. 10 shows the vertical structure of the two terms in the integrand of (40) as well as their sum for these three representative modes. The results verify that the net energy conversion takes place primarily (1) in the heating layer for the modified Eady mode (Fig. 10a), (2) only above the heating layer for the diabatically-induced upper mode (Fig. 10b), and (3) mainly below $p=0.8$ for the diabatically-induced lower mode (Fig. 10c). The heating is so strong in this case that it would be misleading to interprete the two parts in (40) as separate contributions from the dynamical and diabatic processes. It is also of interest to note that there can be locally negative values particularly in the second term of the integrand. The abrupt changes near the boundaries of the uniform heating layer are associated with the temperature discontinuity of the perturbation (first derivative of

the streamfunction) at such boundaries. The fact that the values in panel (b) is 200 × larger than those in panel (a) merely stems from our particular choice of normalization of the eigenfunction and therefore has no special significance. It is their structures that have unique meaning.

3.5. *Dependence on the surface moist layer thickness*

The thickness of the surface moist layer in the atmosphere could be substantially different under different circumstances. Therefore, the top of the surface moist layer (p_b) should be regarded as a parameter independent of the bottom level of the heating layer (p_*) in the atmosphere. It would be instructive to determine how the moist baroclinic instability process might depend upon their relative values. Fig. 11 shows the growth rate results for 2 cases with all other parameters fixed to the reference values. Case A has a thick surface moist layer ($p_b = 0.8$) and case B has a negligibly thin moist layer ($p_b = 0.99$) as a contrast to $p_b = 0.9$ in the reference case. The influence of the self-induced heating is expected to be strong in case A because the moisture convergence would be considerably stronger. It is found that the unstable diabatically induced upper and lower modes can even coexist in this case for a wavelength in the neighborhood of 2500 km (Fig. 11a). This means that sufficiently large potential vorticity is induced at the top and bottom of the heating layer that both the upper unstable mode and the lower unstable mode can develop simultaneously in this case. On the other hand, since there is effectively no self-induced heating in case B due to the kinematic constraint of the bottom boundary on the vertical velocity field, the growth rate curve is effectively the same as that of a dry model (Fig. 11b).

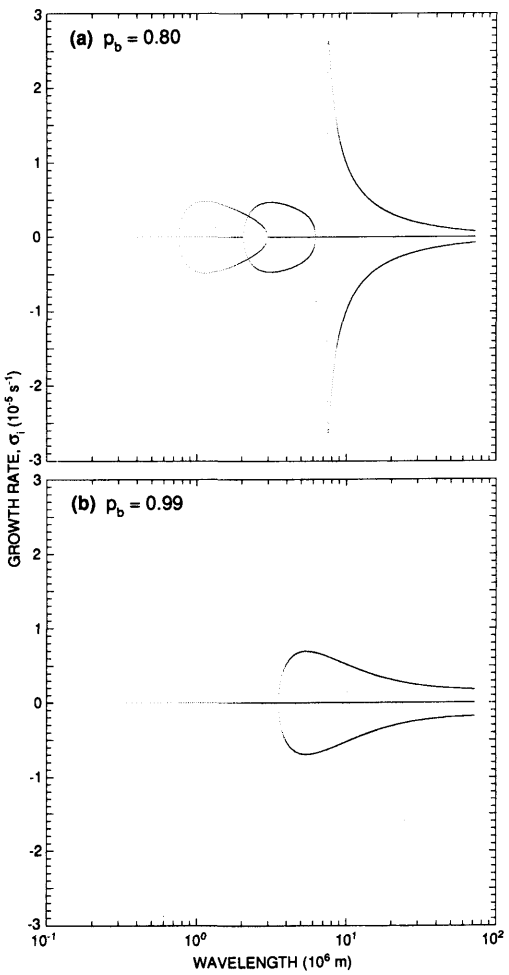

Fig. 11. Variations of the growth rate σ_i of the four eigenmodes with wavelength for the case of (a) a thick surface moist layer, $p_b = 0.80$ and (b) a shallow surface moist layer, $p_b = 0.99$.

4. Concluding remarks

Various specific results are summarized in the Abstract and therefore are not repeated here. The dramatic enhancement of the growth rate and the equally dramatic reduction of the length scale of the most unstable moist Eady mode in a range of moderate values of the heating intensity parameter are manifestations of the strong feedback effects of a self-induced heating process in baroclinic instability. Throughout the text, the results are compared with the counterparts in observation and several numerical model studies wherever available. They are found to be generally compatible.

It is specifically demonstrated in this article that the dynamical nature of moist baroclinic instability can be quite understandable on the basis of what we already know about the dry baroclinic instability. The key consideration is that the heating could give rise to significant local positive or negative potential vorticity (PV) anomalies wherever there is a sharp vertical

gradient in the heating rate, although there is no net change of the PV in a column. When such effects are sufficiently strong as highlighted by the use of a top-hat heating profile with a strong heating, those internal levels play a similar dynamical role as the model surface and tropopause in the Eady model. It would give rise to new unstable modes due to the interaction of the PV anomalies at those discrete levels. The structure of such modes are quite different from that of a moist Eady mode (Fig. 5a) depending on the wavelength (Fig. 5b). The latter are either confined above or below the heating layer. The steering levels of these unstable modes are approximately at the mid-levels of the two corresponding sublayers. Those modes owe their existence to both the basic baroclinic shear and the self-induced heating. These modes may be relevant to some of the short waves observed in the upper troposphere or the relatively small shallow storms in the lower troposphere. It warrants to make a follow-up analysis of them with a more realistic model. It is also pertinent to note that none of the unstable modes over the extensive range of heating in this analysis primarily arises from the interaction of the two PV anomalies induced at the top and bottom of the heating layer as suggested by Snyder and Lindzen (1991). In other words, the dynamical influence of the surface or the tropopause in the model is always of first order importance in moist baroclinic instability in a plausible atmospheric setting. Extension of this analysis in a realistic framework using observed time mean flow is being investigated.

5. Acknowledgment

The support from the National Science Foundation under Grant ATM91-08520 for this research is gratefully acknowledged. Useful comments from Dr. Erland Källen are appreciated.

REFERENCES

Bannon, P. R. 1986. Linear development of quasi-geostrophic baroclinic disturbances with condensational heating. *J. Atmos. Sci.* **43**, 2261–2274.

Bennets, D. A. and Hoskins, B. J. 1979. Conditional symmetric instability, a possible explanation for frontal rainbands. *Quart. J. R. Met. Soc.* **105**, 945–962.

Bonatti, J. P. and Rao, V. B. 1987. Moist baroclinic instability in the development of north Pacific and South American intermediate-scale disturbances. *J. Atmos. Sci.* **44**, 2657–2667.

Bretherton, F. P. 1966. Baroclinic instability and the short wavelength cut-off in terms of potential vorticity. *Quart. J. R. Met. Soc.* **92**, 335–345.

Charney, J. G. and Eliassen, A. 1964. On the growth of the hurricane depression. *J. Atmos. Sci.* **21**, 68–75.

Craig, G. and Cho, H.-R. 1988. Cumulus heating and CISK in the extratropical atmosphere, Part I. Polar lows and comma clouds. *J. Atmos. Sci.* **45**, 2622–2640.

Craig, G. and Cho, H.-R. 1992. Cumulus convection and CISK in midlatitudes, Part II. Comma-cloud formation in cyclonic shear regions. *J. Atmos. Sci.* **49**, 1318–1333.

Emanuel, K. A., Fantini, M. and Thorpe, A. J. 1987. Baroclinic instability in an environment of small stability to slantwise moist convection, Part I. Two-dimensional models. *J. Atmos. Sci.* **44**, 1559–1573.

Fantini, M. 1993. A numerical study of two-dimensional moist baroclinic instability. *J. Atmos. Sci.* **50**, 1199–1210.

Gall, R. L. 1976. The effects of released latent heat in growing baroclinic waves. *J. Atmos. Sci.* **33**, 1686–1701.

Grønås, S., Kvamsto, N. G. and Raustein, E. 1991. Dynamical aspects of the mesoscale storm over northern Germany 27–28 August 1989. *Meteor. Report Series*, University of Bergen, 1992, *Tellus*, submitted.

Gyakum, J. R. 1983. On the evolution of the QE II storm, II. Dynamic and thermodynamic structure. *Mon. Wea. Rev.* **111**, 1156–1173.

Hoskin, B. J. and Berrisford, P. 1988. A potential vorticity perspective of the storm of 15–16 October 1987. *Weather* **43**, 122–129.

Haynes, P. H. and McIntyre, M. E. 1987. On the evolution of vorticity and potential vorticity in the presence of diabatic heating and functional and other forces. *J. Atmos. Sci.* **44**, 828–841.

Kristjansson, J. E. 1990. Model simulation of an intense meso-beta scale cyclone. The role of condensation parameterization. *Tellus* **42A**, 78–91.

Kuo, H. L. 1974. Further studies of parameterization of the influence of cumulus convection on large-scale flow. *J. Atmos. Sci.* **31**, 1232–1240.

Kuo, Y. H., Shaprio, M. A. and Donall, E. G. 1991. The interaction between baroclinic and diabatic processes in a numerical simulation of a rapidly intensifying extratropical marine cyclone. *Mon. Wea. Rev.* **119**, 368–384.

Mak, M. 1982. On moist quasi-geostrophic baroclinic instability. *J. Atmos. Sci.* **39**, 2028–2037.

Moorthi, S. and Arakawa, A. 1985. Baroclinic instability with cumulus heating. *J. Atmos. Sci.* **42**, 2007–2031.

Nakamura, N. 1988. Scale selection of baroclinic instability, effects of stratification and nongeostrophy. *J. Atmos. Sci.* **45**, 3253–3267.

Ooyama, K. 1964. A dynamical model for the study of tropical cyclone development. *Geophis. Intern.* (Mexico) **4**, 187–198.

Robinson, W. A. 1989. On the structure of potential vorticity in baroclinic instability. *Tellus* **41A**, 275–284.

Sardie, J. M. and Warner, T. T. 1983. On the mechanism for the development of polar lows. *J. Atmos. Sci.* **40**, 869–881.

Snyder, C. and Lindzen, R. S. 1991. Quasi-geostrophic wave-CISK in an unbounded baroclinic shear. *J. Atmos. Sci.* **48**, 76–86.

Sundqvist, H., Berge, E. and Kristjansson, J. E. 1989. Condensation and cloud parameterization studies with a mesoscale numerical weather prediction model. *Mon. Wea. Rev.* **117**, 1641–1657.

Tang, C.-M. and Fichtl, G. H. 1983. The role of latent heat release in baroclinic waves, without β-effect. *J. Atmos. Sci.* **40**, 53–72.

Wang, B. and Barcilon, A. 1986. Moist stability of a baroclinic zonal flow with conditionally unstable stratification. *J. Atmos. Sci.* **43**, 705–719.

Whitaker, J. S., Uccellini, L. W. and Brill, K. F. 1988. A model-based diagnostic study of the rapid development phase of the Presidents' cyclone. *Mon. Wea. Rev.* **116**, 2337–2365.